flux is of interest, the superposition of conduction and radiation gives reasonably good results,

$$\vec{q}(x, 0) = 3N\,\nabla\chi(x, 0, N \to \infty) + \tfrac{4}{3}\nabla\chi(x, 0, N \to 0). \quad (8)$$

DISCUSSION

It may be noted in Fig. 4 that in order to maintain the prescribed surface temperatures, heat is to be applied along a part of the surfaces at $x, y = 0$ and removed along the remainder. For $N > 1{\cdot}0$ (conduction predominating), heat flows into the medium along the entire hotter surfaces. The theoretical basis of the linearization procedure was discussed for one-dimensional problems in [3] where it was shown that the radiation-potential profile is not sensitive to the variation of N. For the present two-dimensional problem, calculated curves of $\chi + 3NT$, the radiation potential, exhibit the same character, i.e. their shapes do not change greatly with N, and consequently the success of the linearization is assured.

Further discussions pertaining to the effects of absorption and re-emission on the temperature field can be made by rewriting (1) in the form,

$$\nabla^2 T = -\frac{1}{N}(\phi - T^4) \quad (9)$$

where ϕ and T^4 represent, respectively, the radiant energy absorbed and re-emitted [3]. Obviously, the temperature will be higher than that of pure conduction for $\phi > T^4$ and lower for $\phi < T^4$. It is seen from Fig. 3 that re-emission predominates over absorption only in a small region near the hotter corner, and the latter is more important than the former in a large part of the medium. At smaller values of N, the difference between absorption and re-emission is magnified and hence the larger is the difference between the actual temperature and that of pure conduction. Presumably, the linearization procedure may apply as well when the convective process is involved and an approximate solution of (7) by variational method could be developed.

REFERENCES

1. L. Viskanta and R. L. Grosh, Heat transfer by simultaneous conduction and radiation in an absorbing medium, *J. Heat Transfer* **84C**, 63–72 (1962).
2. Y. P. Chang, A potential treatment of energy transfer in a conducting, absorbing and emitting medium, *ASME paper* No. 67-WA/HT-40.
3. Y. P. Chang and C. H. Kang, Transient and steady heat transfer in a conducting and radiating medium, to appear in *AIAA Jl* and Y. P. Chang and R. S. Smith, Steady and transient heat transfer by radiation and conduction in a medium bounded by two co-axial cylindrical surfaces, *Int. J. Heat Mass Transfer* **13**, 69–80 (1970).
4. P. M. Morse and H. Feshback, *Method of Theoretical Physics*, Chapter 7. McGraw-Hill, New York (1953).

Int. J. Heat Mass Transfer. Vol. 13, pp. 1243–1248. Pergamon Press 1970. Printed in Great Britain

DIFFUSE FREE CONVECTION IN A JET ABOVE AN AXIALLY SYMMETRIC ORIFICE DURING HYDROGEN OUTFLOW INTO AMBIENT AIR

K. BRODOWICZ
Technical University of Warsaw, Poland

(*Received* 26 *September* 1967)

NOMENCLATURE

- x, vertical co-ordinate and orifice axis of symmetry;
- y, horizontal co-ordinate in the plane considered;
- z, horizontal co-ordinate;
- r, horizontal polar co-ordinate, $r^2 = y^2 + z^2$;
- S, displacement of interferometer fringes;
- n, refractive index of gas;
- β, concentration coefficient of volumetric expansion;
- C, volume concentration of hydrogen in air;
- D, diffusivity;
- V_{H_2}, volumetric flow rate of hydrogen;
- Gr, Grashof number for mass transfer;
- Sc, Schmidt number;
- Θ, concentration difference;
- h, dimensionless concentration function;
- ρ, density;
- g, gravitational acceleration;
- ν, kinematic viscosity.

INTRODUCTION

Diffusive free convection in a jet produced by hydrogen outflow into ambient air is characterized by velocity and concentration fields. Boundary conditions of the field depend on the outflow geometry.

The communication presents experimental results on a jet above an orifice, 2·3 mm in diamter, with the axis of symmetry colinear with the vector of the gravity field. Outflow of hydrogen into the ambient air is caused by Archimedes forces alone. Upon leaving the orifice, hydrogen mixes with the air that gives rise to the jet.

Geometry of the orifice and its location in the gravity field suggests an axi-symmetrical jet with the axis of symmetry colinear with the orifice axis, velocity and concentration being symmetrical with respect to this axis. The present investigation explains why the jet is unsteady. It is also found that the jet undergoes periodic changes even though every precaution is taken to protect it from outside perturbations. It must be noted that the symmetry occurs only at certain moments of time. The change which takes place in the velocity field is shown in three photographs representing trajectories of fine dust particles.

The fact that the jet is unsteady makes the investigations extremely difficult. To avoid these difficulties, the present author has adopted the measuring procedure in which the time of measurement is much shorter than the period required for the field to change. However, in a nonsymmetrical case, the measurements of the velocity field are valid only in that plane where they are obtained and the interferogram does not describe the field as a whole.

EXPERIMENTAL METHODS

The velocity field was found by the method described in [1]. The procedure consisted of photographing the trajectories of small particles from which both components of a two-dimensional velocity field are determined in one plane. Measurements were taken in a plane x–y parallel to the axis of symmetry of the orifice

The concentration field was obtained by a Mach–Zehnder interferometer. The interferograms register all changes in the optical properties of the gases with hydrogen concentration in the air occurring in the path of the light beam. Since light passes transversely through the jet, it means that any beam of light goes through areas of different concentrations. Therefore, for determination of concentration from the interferogram, it is necessary to solve the integral equation of the interferometer which in the case considered is possible only for axial symmetry of the jet. In the experiments four identical slots were used to get readable displacements of interferometric fringes. The slots were placed in a line in the path of a light beam at distances larger than the cross-section of the jet.

BEHAVIOUR OF REAL JET

As mentioned above, the jet may undergo periodical changes with time and therefore each of the measured quasi-stable fields is different.

For the analysis, velocity measurements were mainly used since the velocity field may be determined more precisely than the concentration field. Besides, the necessity to solve an integral equation of the interferometer (which is not always possible) makes the procedure very difficult. It is necessary to add that, during the experiment, change of displacement of fringes with time was observed that evidenced that the behaviour of the concentration field was similar to that of the velocity field.

During the experimental measurements of the velocity field, twenty photographs of dust particle trajectories were taken. Three subsequent pictures shown in Fig. 1 illustrate the change of the flow with time while three other pictures presented in Figs. 2a–2c show three different sections of the jet.

The velocity distribution found in the photographs at $x = 4$ cm is drawn in Figs. 3(a) and 3(b) by dashed lines, with u and v taken as the ordinates, respectively. The theoretical data, obtained with assumptions described in the next section of the communication, are presented in the same plots by solid lines.

AXISYMMETRICAL JET

Assumption of axial symmetry has reduced the problem in both fields to a two-dimensional one in the plane parallel to the axis of symmetry of the orifice. The velocity field is presented in Figs. 2(b) and 4 (on a larger scale), the latter consisted of a portion taken from the photograph in Fig. 2 and the upper portion taken from another photograph. Thus, both photographs represent the whole data of the work.

Symmetry in the plane of the photographs is evident and a symmetrical case is treated in the work.

The velocity distributions for different x ($x = 1, 2, 4, 6$ cm) corresponding to Fig. 4 are plotted in Figs. 5(a) and 5(b).

The interferogram shown in Fig. 6 is chosen from a series of interferograms because of the symmetry of fringe displacement.

In this case an assumption is made that the interferogram represents an axisymmetrical jet and the concentration of hydrogen was calculated in the plane x–y. The existing relation between the displacement of fringes $S(y)_x =$ const. and the unknown refractive index under the integral sign is simplified to the integral equation of the Abel type in the axisymmetrical case. The results of the solution obtained in the present work by numerical method described in [2] may be correlated by the relation between the refractive index and the displacement of fringes.

$$\{n_{r_i} = n_{r_i}[S(y_i)]\}_{x=\text{const.}}$$

where r_i is the radius of the pivotal circle in the plane z–y concentric with the axis of symmetry; y_i is the point where the circle r_i crosses the plane x–y, i.e. the y-co-ordinate on the interferogram corresponding to $x =$ const. The change of the refractive index between subsequent circles is linearized by the method adopted.

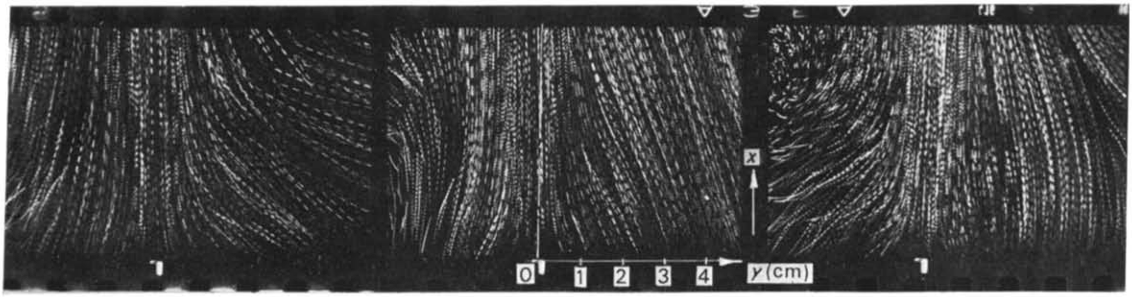

FIG. 1.

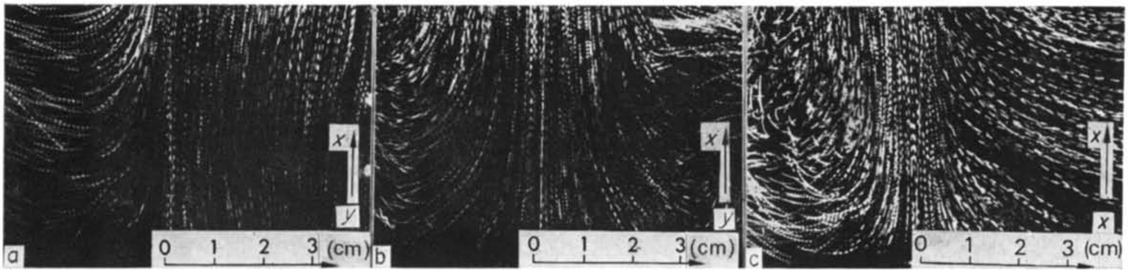

FIG. 2(a).

FIG. 2(b).

FIG. 2(c).

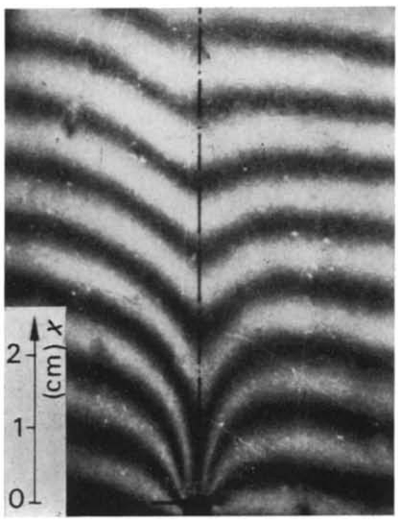

FIG. 6.

[*facing page* **1244**]

FIG. 4.

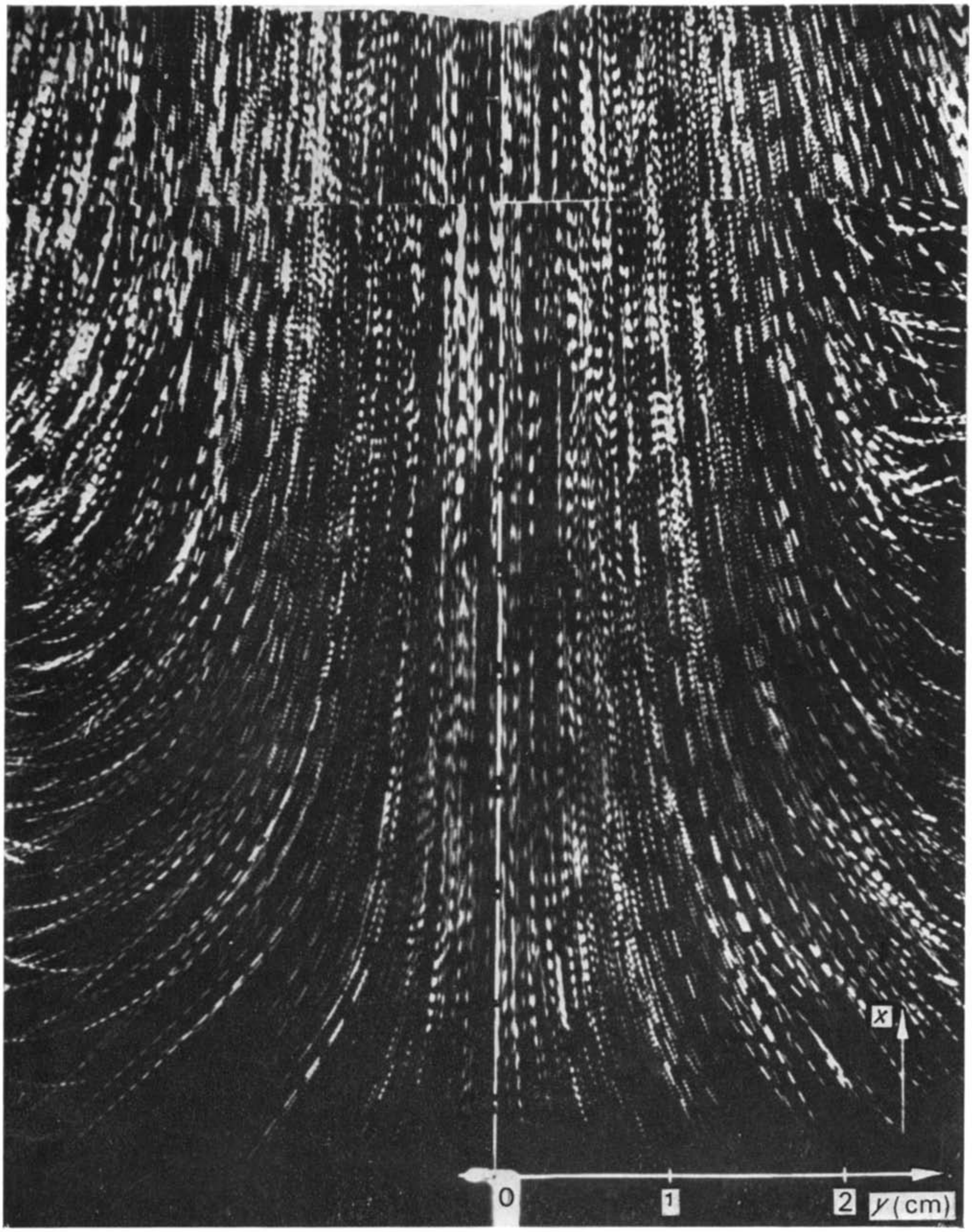

FIG. 4.

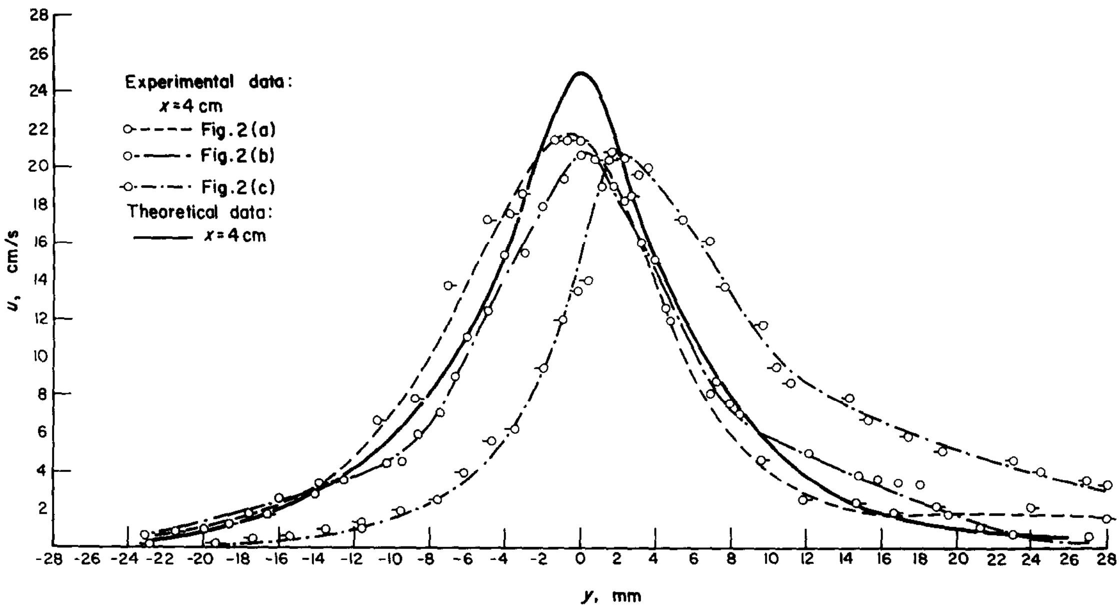
Experimental data:
x=4 cm
Fig. 2 (a)
Fig. 2 (b)
Fig. 2 (c)
Theoretical data:
x=4 cm
u, cm/s
y, mm

FIG. 3(a).

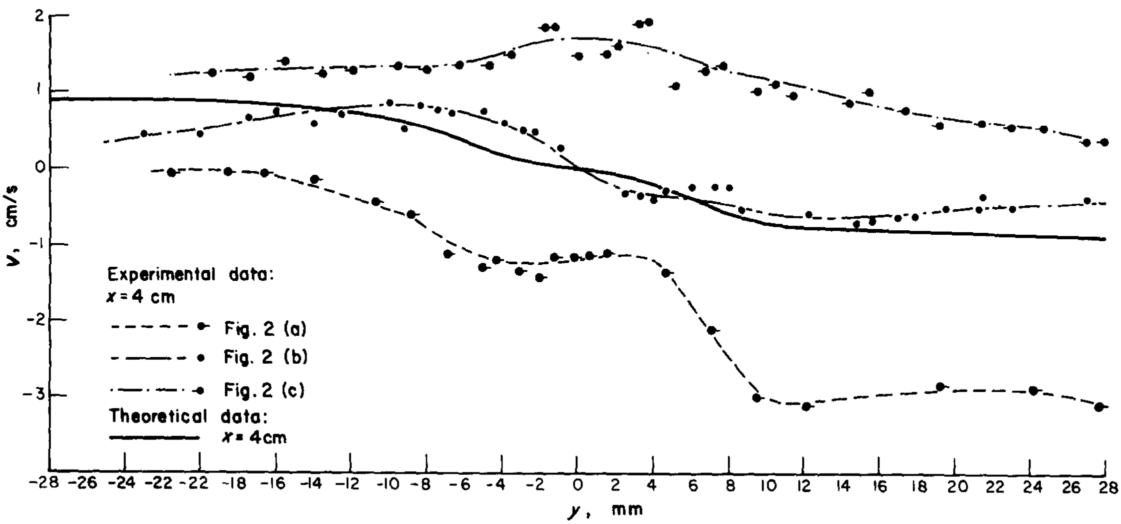
Experimental data:
x=4 cm
Fig. 2 (a)
Fig. 2 (b)
Fig. 2 (c)
Theoretical data:
x=4cm
v, cm/s
y, mm

FIG. 3(b).

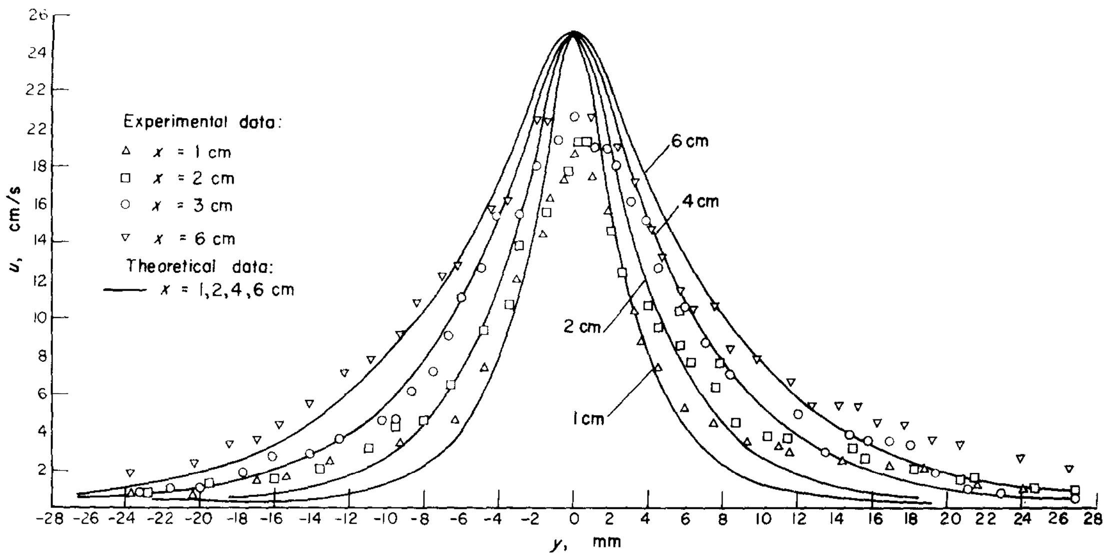

FIG. 5(a).

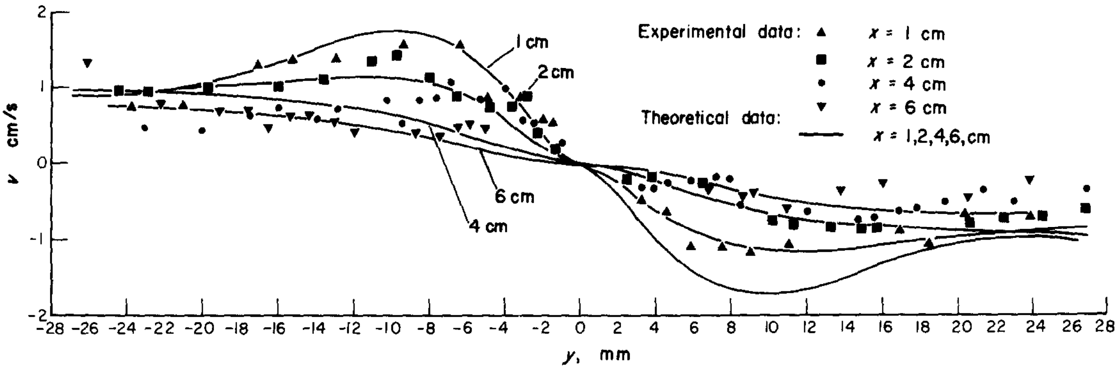

FIG. 5(b).

Table 1.

$x = 1$ cm			$x = 2$ cm			$x = 4$ cm			$x = 6$ cm		
y (mm)	$S(y)$	$C(y)$	y (mm)	$S(y)$	$C(y)$	y (mm)	$S(y)$	$C(y)$	y (mm)	$S(y)$	$C(y)$
19·8	0	0	21·6	0	0	22·4	0	0	22·4	0	0
16·5	0·01	0·28	18·0	0·01	0·30	18·7	0·01	0·28	18·7	0·02	0·49
13·2	0·03	0·70	14·4	0·03	0·64	14·9	0·04	1·00	14·9	0·04	0·91
9·9	0·07	1·61	10·8	0·07	1·54	11·3	0·07	1·22	11·3	0·08	1·23
6·6	0·14	3·78	7·2	0·14	3·45	7·5	0·12	2·66	7·5	0·12	2·26
3·3	0·28	9·87	3·6	0·24	6·45	3·7	0·18	4·50	3·7	0·15	2·95
0	0·50	30·10	0	0·38	18·00	0	0·23	6·80	0	0·17	3·78

The relation between the refractive index of gas and the concentration of hydrogen in the air may be expressed by a linear function of the dependence on the properties of the components and laboratory conditions (756 mm Hg, 22°C).

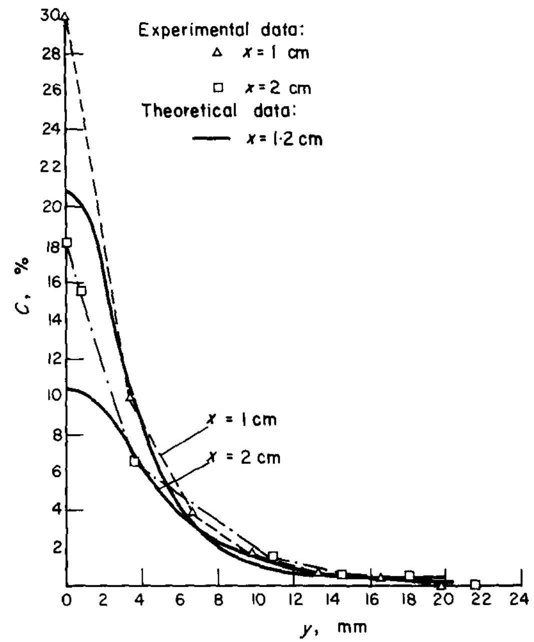

FIG. 7(a).

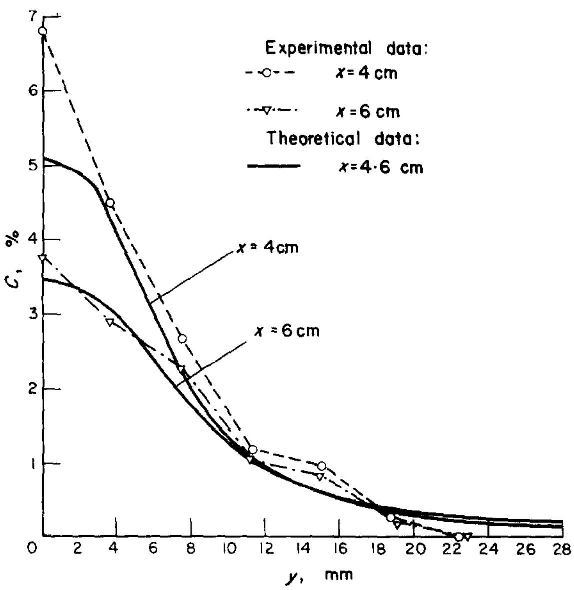

FIG. 7(b).

Hydrogen concentrations in the air pivotal points are shown in Table 1 and plotted in Figs. 7(a) and 7(b) by dotted-dashed lines. On the basis of the determined distribution of concentration and longitudinal velocity component, the volumetric flow rate of hydrogen was calculated by the balance of hydrogen described by the relation

$$V_{H_2} = 2\pi \int_0^\infty uCr\,dr.$$

The values of this integral determined graphically for several values of parameter x are presented in Table 2. Some discrepancies between them may be attributed to the experimental accuracy, and a value of 1·32 cm^3/s may be chosen as the arithmetic mean.

Table 2.

x (cm)	1	2	4	6
V_{H_2} (cm^3/s)	1·32	1·40	1·29	1·28

The mathematical model of the experimentally investigated case is an axisymmetrical laminar jet above a point mass source with constant mass flux and with constant gas properties. The following set of partial differential equations represents this model

$$u\frac{\partial u}{\partial x} + v\frac{\partial u}{\partial y} = g\beta C + \nu\frac{1}{y}\frac{\partial}{\partial y}\left(y\frac{\partial u}{\partial y}\right)$$

$$\frac{\partial}{\partial x}(yu) + \frac{\partial}{\partial y}(yv) = 0$$

$$u\frac{\partial C}{\partial x} + v\frac{\partial C}{\partial y} = D\frac{1}{y}\frac{\partial}{\partial y}\left(y\frac{\partial C}{\partial y}\right)$$

with the boundary conditions

$$y = 0:\quad v = 0;\qquad \frac{\partial u}{\partial y} = 0;\qquad \frac{\partial C}{\partial y} = 0.$$

$$y = \infty:\quad u = 0;\qquad C = 0.$$

Substitution similar to that of Fujii for a point heat source [3]

$$\xi = Gr^{\frac{1}{4}}\frac{y}{x},\quad u = Gr^{\frac{1}{2}}\frac{\nu}{x}\frac{f'}{\xi},\quad C = \Theta h,$$

where

$$Gr = x^3 g\beta\,\Theta/\nu^2,\quad \Theta = V_{H_2}/2\pi\nu x,$$

$$\beta = -\frac{1}{\rho}\left(\frac{\partial\rho}{\partial C}\right)_{P,I} = 0{\cdot}91$$

reduces the partial differential equations to the set of ordinary differential equations

$$f'''\xi^2 + f''f\xi - f'f - f'' + f' + h\xi^3 = 0$$

$$h''\xi + h' + Sc(f'h + h'f) = 0$$

with boundary conditions

$$\xi = 0: \quad f = 0, \quad f'' = 0, \quad h' = 0.$$

$$\xi = \infty: \quad h = 0, \quad f' = 0.$$

Solution of this set of equations, obtained by interpolation for a hydrogen–air mixture with $Sc = 0{\cdot}22$, was taken from [4].

REFERENCES

1. K. BRODOWICZ and W. T. KIERKUS, Determination of streamlines and velocity components in free convection, *Archiwum Budowy Maszyn* **4**, 473–486 (1965).
2. R. W. LADENBURG (Editor), *Physical Measurements in Gas Dynamics and Combustion*. Oxford University Press, Oxford (1955).
3. T. FUJII, Theory of steady laminar natural convection above a horizontal line heat source and point heat source, *Int. J. Heat Mass Transfer* **6**, 597–606 (1963).
4. H. UEHARA and T. FUJII, Natural convection above a horizontal line heat source and a point heat source. Rep. No. 38 of University of Kyushu, Institute of Production Technology, pp. 1–88 (1964).